PHYSICAL REVIEW B VOLUME 54, NUMBER 18 1 NOVEMBER 1996-II

Doping and van Hove singularity dependence of Raman background in $d_{x^2-y^2}$ superconductors

D. Branch and J. P. Carbotte
Department of Physics and Astronomy, McMaster University Hamilton, Ontario, Canada L8S 4M1

(Received 24 August 1995; revised manuscript received 6 May 1996)

In a two-dimensional band-structure model, the effect of doping on the Raman electronic background of a superconductor with $d_{x^2-y^2}$ gap symmetry is studied. Emphasis is placed near optimum doping and on the role of the van Hove singularity. The relationship between peaks in the Raman spectrum for three often discussed photon geometries and the gap is studied. No simple relationship exists, although the B_{1g} mode can show many of the features of the quasiparticle density of states. [S0163-1829(96)03842-8]

I. INTRODUCTION

The broad featureless background electronic Raman continuum observed in the high-T_c oxides[1–5] is found to readjust its intensity as a function of frequency in the superconducting state leading to the appearance of gaplike features.[4–14] Such features have recently been interpreted in terms of a superconducting energy gap with $d_{x^2-y^2}$ symmetry.[9] The theory of Raman scattering in metals is well developed.[15–25] Klein and Dierker[17] showed that the Raman vertices in varying photon polarization geometries can lead to different Raman spectra in anisotropic superconductors. In a recent publication,[25] the present authors gave results of calculations of the electronic Raman-scattering susceptibility for the B_{1g}, B_{2g}, and A_{1g} photon geometries in a d-wave superconductor. The Raman vertices were calculated from a realistic two-dimensional band structure used to model the copper-oxide plane. The electron pairing was assumed to proceed through the antiferromagnetic spin-fluctuation model of Millis, Monien, and Pines (MMP).[26] The superconducting state was characterized through numerical solutions of the BCS gap equations using fast-Fourier-transform methods. In this article, we follow the same procedure, extending our previous work to study doping effects. Particular emphasis is placed on the rule of the van Hove singularity. When the van Hove singularity falls at the Fermi surface, the critical temperature will be maximum (optimum doping). In our work, we fit the only parameter entering the gap equation, namely the strength of the electron coupling to the spin susceptibility, so as to get a $T_c = 100$ K at optimum doping which is a value that can be taken as characteristic of the oxides. Once a band structure is specified, there remains no adjustable parameters and the gap follows. In all our numerical solutions, we find $d_{x^2-y^2}$ symmetry although many higher-order harmonics are present besides the lowest one for the $d_{x^2-y^2}$ irreducible representation of the two-dimensional tetragonal point group of the CuO_2 lattice.

In Sec. II, we present the necessary formalism and discuss results for the quasiparticle density of state. Section III contains our numerical results for the Raman scattering as well as some discussion of these results. In Sec. IV, we draw conclusions.

II. FORMALISM AND T_c VALUE

The Raman cross section is related to the Raman response function $\chi_{\Gamma\gamma}$ given by[15–25]

$$\chi_{\Gamma\gamma}(q;i\nu_n) = -T\sum_{\mathbf{k}} \mathrm{tr}\{\hat{\Gamma}(\mathbf{q}+\mathbf{k};i\nu_n)G(\mathbf{q}+\mathbf{k};i\nu_n + i\omega_m)\hat{\gamma}(\mathbf{k})G(\mathbf{k};i\omega_m)\}, \tag{1}$$

where tr stands for trace, ω_n (ν_n) is the fermion (boson) Matsubara frequency given by $[2n+1]\pi T$ ($2n\pi T$) with T the temperature in energy units and $n=0, \pm 1, \pm 2, \ldots$. In Eq. (1), $\hat{\Gamma}(\mathbf{k};i\nu_n)$ and $\hat{\gamma}(\mathbf{k})$ are, respectively, dressed and bare Raman vertices which are 2×2 matrices. In terms of the Pauli matrices τ, the bare vertex $\hat{\gamma}(k)=\gamma(\mathbf{k})\tau_3$ is

$$\gamma(\mathbf{k}) = \sum_{\alpha\beta} e^I_\alpha \frac{\partial^2 \epsilon_{\mathbf{k}}}{\partial k_\alpha \partial k_\beta} e^s_\beta, \tag{2}$$

where $\mathbf{e}^I(\mathbf{e}^s)$ is the initial (scattered) photon polarization vector and $\epsilon_{\mathbf{k}}$ is the electron energy dispersion so that the second derivative of ϵ_k in Eq. (2) is the inverse of the effective mass tensor. For a two-dimensional copper-oxide plane, we will take for $\epsilon_{\mathbf{k}}$, the form

$$\epsilon_{\mathbf{k}} = -2\overline{t}\{[\cos(k_x a)+\cos(k_y a)] - 2B\cos(k_x a)\cos(k_y a) - (2-2B-\mu)\}, \tag{3}$$

where $\overline{t}$ is the first-nearest-neighbor hopping and B is the second-nearest-neighbor in units of $\overline{t}$. In Eq. (3), a is the lattice parameter in the square lattice and can be taken to be 1 in dimensionless units. Finally, μ is the chemical potential.

In Eq. (1), $G(\mathbf{k};i\omega_n)$ is the 2×2 Nambu Green's function given by

$$G(\mathbf{k};i\omega_n) = -\frac{i\omega_n\tau_0 + \epsilon_{\mathbf{k}}\tau_3 + \Delta_{\mathbf{k}}\tau_1}{\epsilon^2_{\mathbf{k}} + \Delta^2_{\mathbf{k}} + \omega^2_n}, \tag{4}$$

where $\Delta_{\mathbf{k}}$ is the gap in the superconducting state. Finally, the dressed Raman vertex in Eq. (1) is to satisfy the equation[17]

$$\hat{\Gamma}(\mathbf{q};i\nu_n) = \hat{\gamma}(\mathbf{q}) - T\sum_{m,\mathbf{k}} \mathrm{tr}\{\hat{\Gamma}(\mathbf{k}+\mathbf{q};i\nu_n+i\omega_m) \times G(\mathbf{q}+\mathbf{k};i\nu_n+i\omega_m)V(\mathbf{q};i\nu_n)G(\mathbf{k};i\omega_m)\}. \tag{5}$$

For a static screened Coulomb potential $V(\mathbf{q};i\nu_n)$ to lowest order in $\mathbf{q}$, i.e., $\mathbf{q}\to 0$, we can write (a result given by Klein and Dierker)[17]

0163-1829/96/54(18)/13288(7)/$10.00

$$\chi_{\Gamma\gamma}(q;i\nu_n)=\chi_{\gamma\gamma}(q;i\nu_n)-\frac{\chi_{\gamma 1}(\mathbf{q};i\nu_n)\chi_{1\gamma}(\mathbf{q};i\nu_n)}{\chi_{11}(\mathbf{q};i\nu_n)},\tag{6}$$

where $\chi_{\gamma\gamma}$ is given by Eq. (1) with $\hat{\Gamma}$ replaced by $\hat{\gamma}$, $\chi_{1\gamma}$ with $\hat{\Gamma}$ replaced by 1, $\gamma_{\gamma 1}$ with $\hat{\Gamma}$ replaced by $\hat{\gamma}$ and $\hat{\gamma}$ replaced by 1; and χ_{11} with both $\hat{\Gamma}$ and $\hat{\gamma}$ replaced by 1. The response function $\chi_{\gamma\gamma}(\mathbf{q};i\nu_n)$ can be worked out from the definition of the Green's function (4) (β is the inverse temperature) to be

$$\chi_{\gamma\gamma}(q\to;i\nu_n)=-\frac{4}{\Omega}\sum_{\mathbf{k}}\frac{|\gamma_{\mathbf{k}}|^2\Delta_{\mathbf{k}}^2}{E_{\mathbf{k}}[4E_{\mathbf{k}}^2+\nu_n^2]}\tanh\left(\frac{\beta E_{\mathbf{k}}}{2}\right),\tag{7}$$

where $E_{\mathbf{k}}\equiv\sqrt{\epsilon_{\mathbf{k}}^2+\Delta_{\mathbf{k}}^2}$ and Ω is the volume. Similar expressions hold for $\chi_{\gamma\gamma}$, $\gamma_{1\gamma}$, and γ_{11} in which one or both factors of $\gamma_{\mathbf{k}}$ in Eq. (7) are replaced by 1. The Raman-scattering cross section then follows from the analytic continuation of Eq. (6) to the real frequency axis through the analytic continuation $i\nu_n\to\omega+i0^+$. Because of symmetry, $\chi_{\gamma 1}$ vanishes for the B_{1g} and B_{2g} modes but is finite for the A_{1g} mode so Coulomb effects only renormalize the A_{1g} channel. For the other two channels, the simpler expression (7) applies, and we are only interested in the imaginary part of Im $\chi_{\gamma\gamma}(\mathbf{q}=0;i\nu_n=\omega+i0^+)$ which we will denote by Im $\chi_{\gamma\gamma}(\omega)$. We will use this same notation even when a Coulomb renormalization [see Eq. (6)] is applied.

To proceed, we need some model for the gap $\Delta_{\mathbf{k}}$ as a function of momentum in the first Brillouin zone of the two-dimensional copper-oxide plane. Here we will use the same procedure as in our previous work.[25] To be definite, we solve a BCS gap equation appropriate to the nearly antiferromagnetic Fermi-liquid model of Millis, Monien, and Pines.[26] In this model, the pairing is thought to occur through the phenomenological electron-spin susceptibility[25–33] $\chi_{\mathbf{kk}'}$ given by MMP as

$$\chi_{\mathrm{MMP}}(\mathbf{k}-\mathbf{k}')=\frac{\chi_{\mathbf{Q}}}{1+\delta^2(\mathbf{q}-\mathbf{Q})^2},\tag{8}$$

where δ=2.25 Å, $\chi_Q=10$ states/eV, and the commensurate wave vector $\mathbf{Q}=(\pi/a,\pi/a)$. The BCS equation is

$$\Delta_{\mathbf{k}}=-\frac{1}{\Omega}\sum_{k'}g^2\chi_{\mathrm{MMP}}(\mathbf{k}-\mathbf{k}')\,\frac{\Delta_{k'}}{E_{k'}}\tanh\left(\frac{\beta E_{k'}}{2}\right),\tag{9}$$

where the coupling constant g is arbitrary and varied to get the desired value of the critical temperature. Here we will take T_c to be 100 K, a value representative of the copper-oxide superconductors. No parameters remain in Eq. (9) and a numerical solution by a fast-Fourier-transform technique gives us the momentum-dependent gap function $\Delta_{\mathbf{k}}$. For the model susceptibility given by Eq. (8), the solutions exhibit $d_{x^2-y^2}$ symmetry although they involved a superposition of lowest and many of the higher-order harmonics in this irreducible representation for the two-dimensional copper-oxide tetragonal lattice. We refer the reader to our earlier work for details.[26] Once the gap is known, the Raman cross section Eq. (7) can be calculated. Of course, the results will depend on band structure through our choice of dispersion relation Eq. (3). In Eq. (3), we will take $t=100$ meV and many of our first results will be for $B=0.16$. Later, we will vary B as well. The chemical potential is determined for a given filling $\langle n\rangle$ through the equation[26]

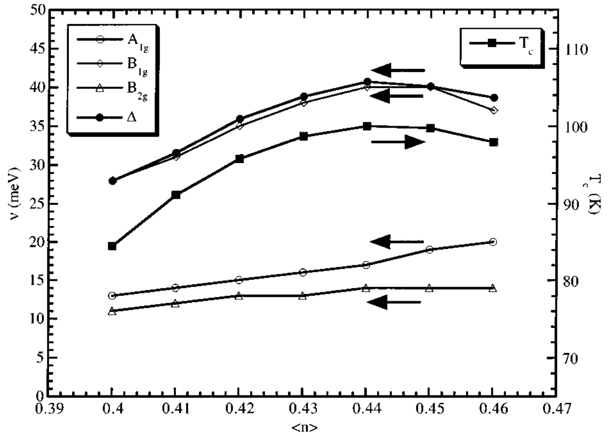

FIG. 1. The critical temperature (solid squares) is plotted as a function of filling for a band structure model with $B=0.16$ and $t=100$ meV. Also plotted are the frequencies (in meV) for maxima in the different Raman geometries. The notation is (○) A_{1g} mode, (◇) B_{1g}, (△) B_{2g}. The solid circles are twice the frequency of the gap maximum in the quasiparticle density of states as shown in Fig. 2.

$$\langle n\rangle=\frac{1}{2}\frac{1}{\Omega}\sum_{\mathbf{k}}\left[1-\frac{\epsilon_{\mathbf{k}}}{E_{\mathbf{k}}}\tanh\left(\frac{E_k}{2k_BT}\right)\right].\tag{10}$$

One of our interests in this paper is an understanding of the role played in the Raman-scattering cross section of the van Hove singularity in the electronic density of state. When the chemical potential μ in Eq. (3) is such that we are near the maximum in the normal-state density of states, the value of the critical temperature is enhanced. This is illustrated in Fig. 1 where T_c is shown as a function of filling $\langle n\rangle$ given by Eq. (10) for $t=100$ meV, $B=0.16$ and g^2 in the BCS equation (9), set so that at $\langle n\rangle=0.44$ the critical temperature has a value of 100 K at optimal doping. On either side of optimum doping, under doped with lower value of $\langle n\rangle$ and overdoped for higher value of $\langle n\rangle$, the value of T_c drops in qualitative agreement with experiment although the precise relationship between doping and filling is not well known and our model is certainly too simple to expect quantitative agreement with experiment. It does, however, allow us to achieve some understanding of the effect of filling on various superconducting properties.

III. NUMERICAL RESULTS

We begin with a discussion of the quasiparticle density of state $N(\omega)$ as a function of energy in the superconducting state. It is given by

$$N(\omega)=\lim_{\Gamma\to 0}\frac{1}{\Omega}\sum_{\mathbf{k}}\frac{\Gamma}{(E_{\mathbf{k}}-\omega)^2+\Gamma^2},\tag{11}$$

where the Lorentzian form is just a convenient representation of a dirac δ functions useful for numerical work on a lattice of finite size. In Fig. 2, we show a series of results for the

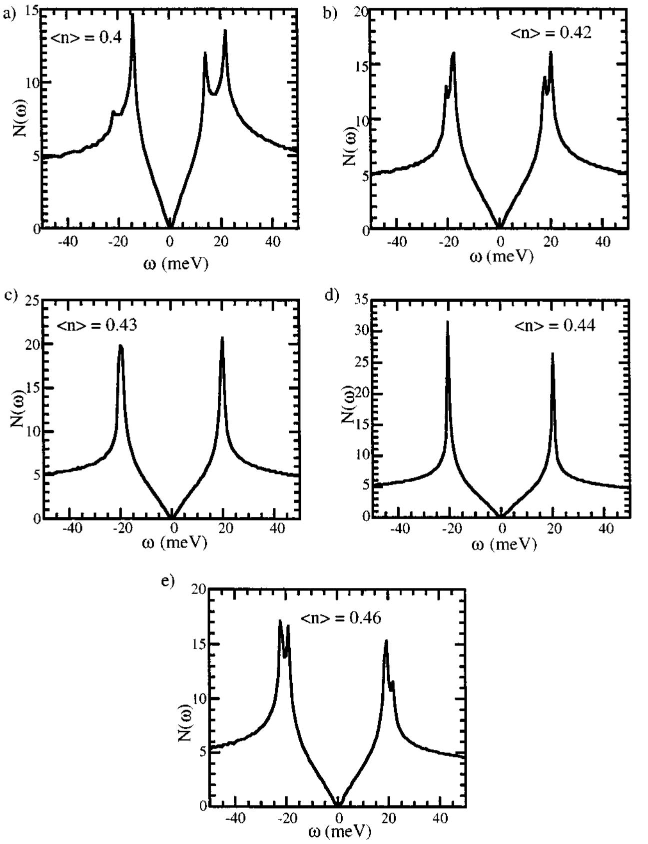

FIG. 2. Quasiparticle density of states $N(\omega)$ in the superconducting state as a function of frequency ω in (meV). In all frames, the next-nearest-neighbor hopping $B=0.16$, nearest-neighbor $t=100$ meV. The filling $\langle n\rangle$ is changed and is 0.4, 0.42, 0.43, 0.44, 0.46 for frames (a)–(e), respectively. The van Hove singularity in the band structure falls at 22 meV for $\langle n\rangle=0.4$.

quasiparticle density of state for five different values of filling in the case $t=100$ meV, $B=0.16$ and T_c at optimum doping equal to 100 K. Frames (a)–(e) are, respectively, for $\langle n\rangle=0.4$, 0.42, 0.43, 0.44, and 0.46. In frame (a) for $\langle n\rangle=0.4$, which falls in the under doped region with a T_c value of about 84 K (see Fig. 1), we note first that the density of state $N(\omega)$ is shown with zero placed right at the Fermi energy (as will be the case for all other frames) and that it rises linearly from zero as ω increases. The first peak, which falls around 13 meV, is the gap peak which is followed by the van Hove singularity peak at about 22 meV.[34] Note that both these features appear on either side of $\omega=0$ in the density of state, but that the figure does not have full inversion symmetry because for $B\neq 0$ the van Hove singularity is not at $\omega=0$. As the filling is increased towards optimum doping, T_c increases and we see in frame (b) that the gap peak has also moved up in energy and is now closer to the van Hove peak than was the case in frame (a). The absolute value of the density of state at maximum has also increased. The effect is even more pronounced in frame (c) for $\langle n\rangle=0.43$ in which case the gap peak and van Hove singularity fall very near each other and are not resolved within the resolution of our numerical work. Note that in our numerics, Γ in Eq. (11) is finite. Both gap and van Hove singularity now fall near 20 meV. At optimum doping $\langle n\rangle=0.44$ [frame (d)], the value of the density of state at maximum has risen to a value of 30 in our units and gap and van Hove peaks fall at the same energy. The final frame (e) is for the overdoped situation with filling $\langle n\rangle=0.46$ and T_c reduced slightly to about 98 K. We see that the position of the gap peak has lowered somewhat from its value in frame (d) for optimum doping and that a second peak due to the van Hove singularity is now resolved. Also, the overall height of the density of state at maximum is reduced in comparison with frame (d).

We now want to trace the effect of the van Hove singularity on the Raman-scattering cross section Im $\chi_{\gamma\gamma}(\omega)$ defined in the previous section and compare this with what we have just learned about the behavior of the quasiparticle density of state. Figure 3(a) shows our results for the case of the B_{1g} channel. As for Figs. 1 and 2, $t=100$ meV, $B=0.16$, and g^2 is fixed by insisting that T_c at optimum doping be 100 K. The filling is changed through optimum doping from $\langle n\rangle=0.4$ (solid curve) to $\langle n\rangle=0.41$ (narrow dashed), $=0.42$ (intermediate dashed dotted), $=0.43$ (short dashed), $=0.44$ (dotted), $=0.45$ (long dashed-triple dotted), and $=0.46$ (long dashed). First note that we predict a single peak at approximately 40 meV for the case of optimum doping (dotted curve), exactly as seen in the quasiparticle density of state [Fig. 2, frame (d)]. The peak is, however, at twice the gap value seen in $N(\omega)$. This is expected since the expression for the Raman cross section can be written in the form [see Eq. (7)]

$$\mathrm{Im}\,\chi_{\gamma\gamma}(\omega)=\frac{1}{\Omega}\,\mathrm{Im}\sum_{\mathbf{k}}\frac{|\gamma_k|^2\Delta_k^2}{E_k^2}\tanh\left(\frac{\beta E_{\mathbf{k}}}{2}\right)\times\left[\frac{1}{2E_k+\omega+i0^+}+\frac{1}{2E_k-\omega-i0^+}\right] \tag{12}$$

with the denominator vanishing for $\omega=\pm 2E_{\mathbf{k}}$ rather than $\omega=\pm E_k$ in the density of state expression (11). When we move off optimum doping on either side, the peak in the Raman intensity is reduced in magnitude, see dashed triple dotted curve with $\langle n\rangle=0.45$ overdoped case and the short dashed curve with $\langle n\rangle=0.43$ slightly under doped case. No second peak is resolved in these two curves. For the long dashed curve with $\langle n\rangle=0.46$ and the intermediate dashed-dotted curve with $\langle n\rangle=0.42$ displaced to either side of optimum doping at $\langle n\rangle=0.44$, a second peak, due to the van Hove singularity at higher energy, is clearly present as it was in $N(\omega)$ and this is even seen more clearly in the last two curves for which $\langle n\rangle=0.40$ (solid) and $\langle n\rangle=0.41$ (narrow dashed). In these curves, the intensity of the Raman profile is lower at the gap maximum than for the other cases and broader in energy with a second maximum clearly seen at higher energy. As we have stressed, this peak has its origin in the van Hove singularity in the electronic density of state of the two-dimensional tight-binding band. It is clear that the Raman electronic background, in principle, will give much the same information as tunneling, a technique which should, in principle, yield $N(\omega)$ although, in practice, there sometimes appears to be severe problems with this method and unambiguous results are not always obtained. This perhaps may be because, in the high-T_c oxides, the coherence length is so short that only a few surface layers are probed and that these are not completely representative of the bulk. While

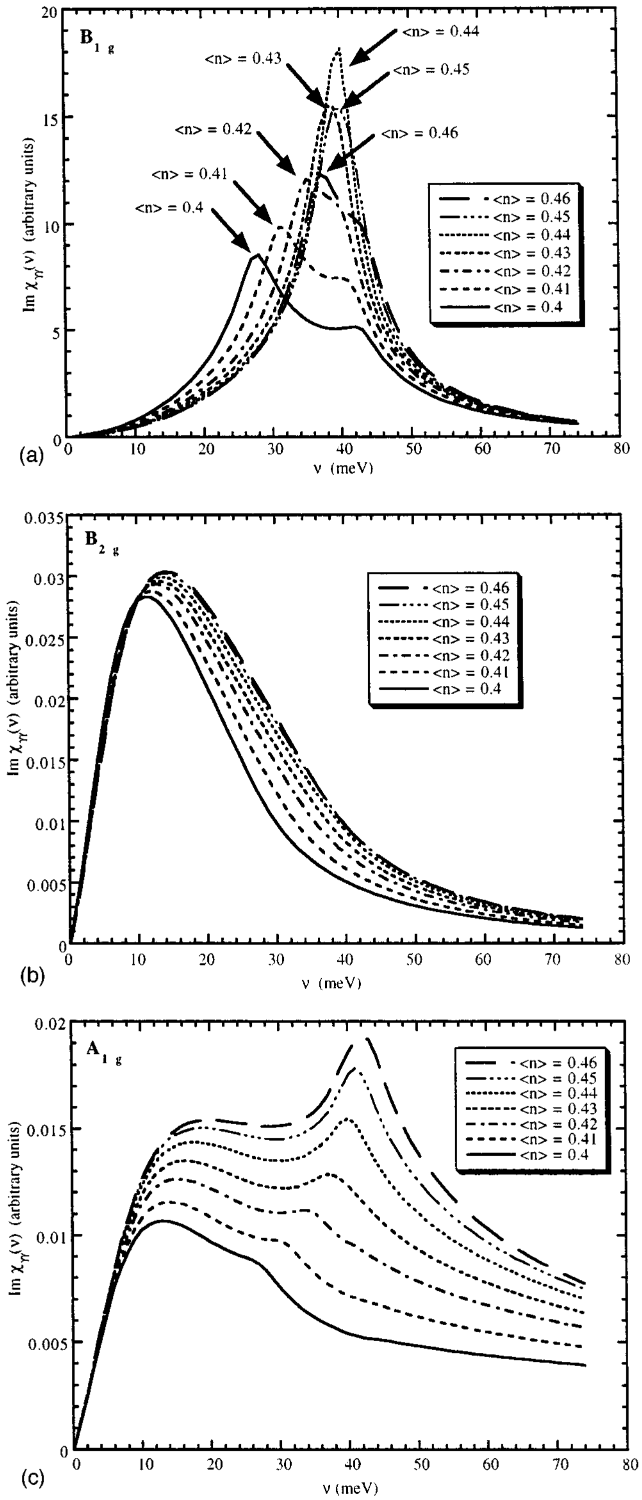

FIG. 3. Raman-scattering cross section as a function of frequency ω in (meV) for the (a) B_{1g}, (b) B_{2g}, and (c) A_{1g} modes. In the calculation, the second-nearest-neighbor hopping $\overline{B}=0.16$ and first neighbor $\overline{t}=100$ meV. The fillings considered are $\langle n\rangle=0.4$ (solid curve), $=0.41$ (narrow-dashed), $=0.42$ (intermediate dashed dotted), $=0.43$ (short dashed), $=0.44$ (dotted) [near optimum doping], 0.45 (long dashed-triple dotted), and 0.46 (long dashed).

the B_{1g} Raman spectrum is very similar in appearance to the density of states, Eq. (12) for Im $\chi_{\gamma\gamma}(\omega)$ and Eq. (11) for the density of states do differ by more than the one having a two-δ, while the other has a one-δ gap feature as we have just described. The Raman profile is further weighted by the vertex factor $|\gamma_{\mathbf{k}}|^2$ which does not appear in the density of states. At zero temperature, the thermal factor in Eq. (12) is, of course, gone. This vertex factor selectively weights certain parts of the Brillouin zone.[25] For a different Raman channel, the vertex $|\gamma_{\mathbf{k}}|^2$ can be quite different and the resulting profile can have a very different shape as seen in Fig. 3(b) where we show results for Im $\chi_{\gamma\gamma}(\omega)$ for the B_{2g} mode as a function of doping with $\langle n\rangle$ ranging from an under doped sample with filling 0.4 to an overdoped one with 0.46. As before $\langle n\rangle=0.4$ (solid line), 0.41 (narrow dashed), 0.42 (intermediate dashed dotted), 0.43 (short dashed), 0.44 (dotted) (near optimum doping), 0.45 (long dashed-triple dotted), and 0.46 (long dashed). In this case, the peak in the Raman profile is not even close to falling at approximately twice the value of the gap peak in the density of states seen in Fig. 2. Also, the curves order simply according to increased doping and show no sign of the decrease in T_c and by implication of gap value for the underdoped and overdoped regime when compared with optimum doping. The maximum of the intensity increases slightly with increasing $\langle n\rangle$ and its position also shifts very slightly towards higher energies. This behavior is completely different from that of the B_{1g} mode which, as we have discussed, reflects much of the properties of the density of states. The B_{2g} mode in no way resembles a density of state curve. For example, there is no trace of the van Hove singularity in Fig. 3(b) yet it is quite prominent in Fig. 3(a) for the B_{1g} mode. The only difference between these two Raman geometries is the vertex factor $|\gamma_{\mathbf{k}}|^2$ in Eq. (12) which obviously can have a profound effect on the resulting profile.

In Fig. 3(c), we show our results for the A_{1g} mode with screening included according to Eq. (6). These profiles, which would look more like those of Fig. 3 for the B_{1g} mode if screening was not included, actually look more like those for the B_{2g} mode except that they are generally lower in intensity and significant in magnitude over a larger energy range. They show a second peak at higher energies besides that around 10–20 meV. As was the case for the B_{2g} mode, the profiles order according to value of filling and do not show a reversal of trends about optimum filling as did the B_{1g} mode of Fig. 3(a). It is clear then that the only spectrum that is easily interpretable as a weighted density of states is the B_{1g} mode.

It is important to note that in our calculations the screening of the A_{1g} mode has reduced its intensity enormously so that it is almost three orders of magnitude smaller than the B_{1g} mode. The screened A_{1g} response, however, is enormously sensitive to the assumed underlying band structure.[38] This suggests that quantitative predictions for a particular material will need to await reliable band information. Here we have presented results for a simple generic band structure and should not be thought of as describing a particular system. To illustrate the sensitivity of the screened A_{1g} to band-structure effects, we consider dispersion relation Eq. (3) with an additional term of the form $C[\cos(2k_xa)+\cos(2k_ya)]$ in the curly brackets. This has been suggested in band-structure calculations[35,36] and angle-resolved photoemission spectroscopy experiments for Y-Ba-Cu-O. In Fig. 4, we compare results for the B_{1g} and A_{1g} modes with filling $\langle n\rangle=0.4$ for a case with $C=0.25$. The dashed curves are for comparison and apply to the case $C=0.0$ previously presented in Fig. 3.

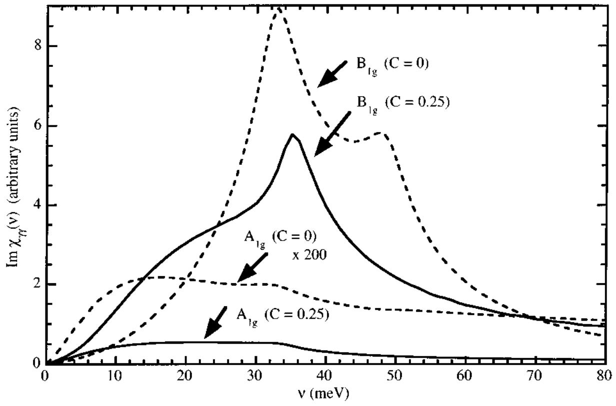

FIG. 4. Comparison of results for the B_{1g} (higher curves) and screened A_{1g} (lower curves) for a band structure with $C=0$ (dashed curves) and $C=0.25$ (solid curves) where c is defined in the text and multiplies a term of the form $\cos(2k_xa)+\cos(2k_ya)$ which is added to the dispersion relation Eq. (3) for the two-dimensional band structure. Note that for the A_{1g} case (lower curve) the dashed curve has been multiplied by a factor of 200.

The solid curves differ only in that $C=0.25$ yet the results are very different. The two upper curves are for B_{1g}. We see that the curves are different in shape but very similar in magnitude. The situation for the A_{1g} mode is completely different. Screening has reduced the intensity of the dashed curve by a factor of almost 1000, while the solid curve is reduced by much less, a factor of about 10. It is clear then that no quantitative predictions[37] of screening effects can be made with confidence at this stage because the details of the band structure of a particular material are not yet confidently established.

We now return to our main theme and all calculations from this point on will be for $C=0$, i.e., the simpler band-structure model of Eq. (3). In Fig. 1, we plot the frequency at the first maximum of the Raman profile as a function of filling $\langle n\rangle$ for the three modes considered in Fig. 3, namely B_{1g} (open diamonds), B_{2g} (open triangles), and A_{1g} (open circles). Also, shown for comparison (solid circles) is the position of twice the frequency at the gap peak in the quasiparticle density of states of Fig. 2. It is quite clear that only the B_{1g} mode reflects fairly directly the information on gap amplitude. The screened A_{1g} and the B_{2g} profiles weight portions of the Fermi surface which overlap the nodes in the $d_{x^2-y^2}$ gap. These spectra are sensitive to excitation in the nodal regions but provide no information on gap amplitude. This is important for the interpretation of data. For completeness, the maximum intensity of Im $\chi_{\gamma\gamma}(\omega)$ is plotted as a function of filling $\langle n\rangle$ in Fig. 5 for four cases, namely B_{1g} (open diamonds), B_{2g} (solid diamonds), A_{1g} with screening (solid circles), and A_{1g} without screening (open circles). Note the different scale on right-hand side for A_{1g} screened and B_{2g} and on the left-hand side for A_{1g} unscreened and B_{1g}. These two cases have a much larger intensity in our calculation than do the other two. We note that the B_{1g} case varies in a similar way to the value of the critical temperature T_c vs $\langle n\rangle$ shown in Fig. 1, while the B_{2g} and screened A_{1g} case do not. They show no trace of a peak at optimum doping and simply increase with increasing value of $\langle n\rangle$. So we can expect no direct correlation between intensity and T_c value in these cases. Again, the general conclusion is that it is only the B_{1g} profile that behaves similarly to a density of states. Some of the features predicted here have not yet been confirmed and some experimental results are in conflict. We now focus further only on this particular case (B_{1g}).

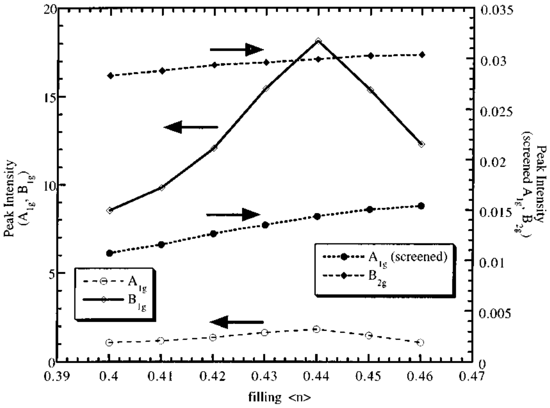

FIG. 5. Intensity of Raman-scattering cross section at maximum as a function of filling $\langle n\rangle$. The notation is (○) A_{1g} mode with no screening, (◇) B_{1g} mode, (●) A_{1g} screened, and (◆) B_{2g}. Right-hand scale applies for A_{1g} screened and B_{2g}, and left-hand scale for A_{1g} unscreened and B_{1g}. Detail line shapes are found in Figs. 3–5.

Based on the dispersion curve of Eq. (3), the bare Raman vertex for the B_{1g} mode is independent of second-neighbor hopping B and is given by

$$\gamma_{\mathbf{k}}^{B_{1g}}=2\overline{t}[\cos(k_x)-\cos(k_y)], \tag{13}$$

which is zero along the two main diagonals and largest at the four points $(0,\pm\pi)$ and $(\pm\pi,0)$. A plot of $|\gamma_{\mathbf{k}}^{B_{1g}}|$ as a function of $\mathbf{k}$ in the first Brillouin zone is shown in Fig. 6(a), while the corresponding constant $|\gamma_{\mathbf{k}}^{B_{1g}}|$ contours are given in frame (b) of the same figure. This holds for any value of B in contrast to the A_{1g} and B_{2g} case in which instance B would enter the Raman vertex. In Fig. 6, we show the Fermi-surface contours for three different values of B, namely $B=0$, $B=0.3$, and $B=0.45$ all at fixed filling set at $\langle n\rangle=0.4$. The integrand in Eq. (12), of course, strongly weights the Fermi contour in the sum over the first Brillouin zone of the two-dimensional copper-oxide plane. For $B=0$, the Fermi contour does not pass close to the $(0,\pm\pi)$, $(\pm\pi,0)$ points where the gap is maximum and where the Raman vertex for the B_{1g} mode is also peaked. As B is increased, the Fermi surface, of course, samples more of this important region. At $B=0.3$ as shown in the figure, the contours are coming in contact with the Brillouin-zone boundary but are already receding from the $(\pm\pi,0)$, $(0,\pm\pi)$ point and this is even more so for the $B=0.45$ case.

We have calculated the Raman cross section for a range of B values, all with the filling $\langle n\rangle$ fixed at 0.4 and the coupling g^2 in the BCS equation adjusted so that T_c is 100 K in all cases so that the maximum gap in the Brillouin should also be roughly the same in each case. Figure 7 shows our results for the position of the gap maximum in the B_{1g} Raman cross section as a function of the second-nearest-neighbor hopping B from 0 to 0.45. We see that this frequency ranges from 30 meV at $B=0$ to take on a maximum

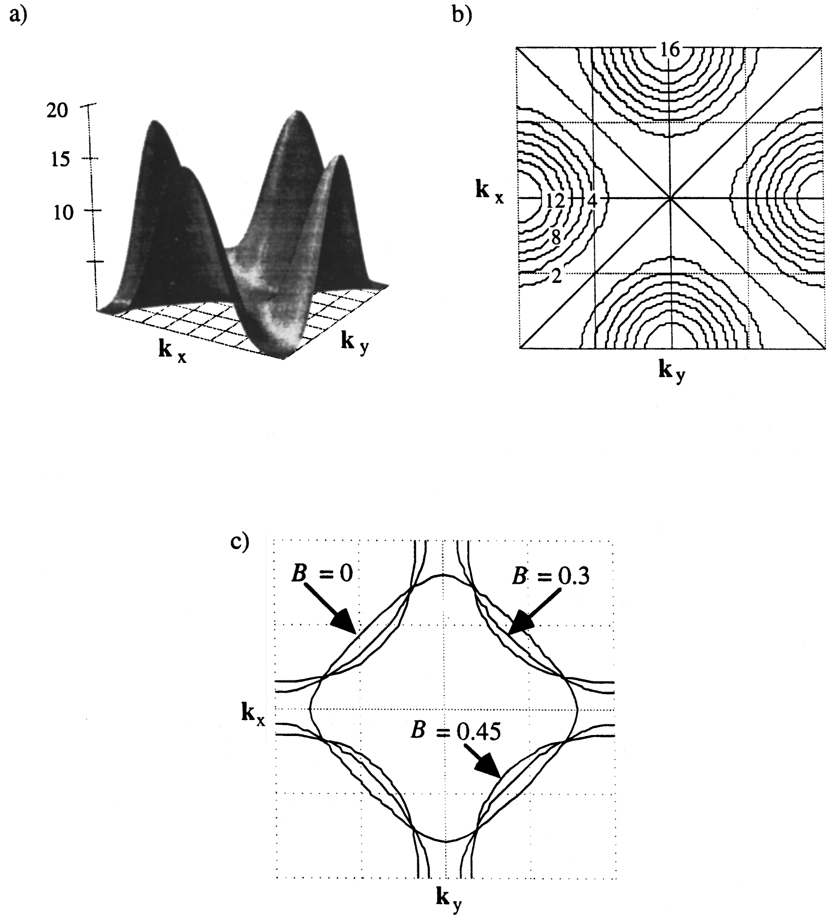

FIG. 6. The square of the Raman vertex $|\gamma_{\mathbf{k}}^{B_{1g}}|^2$ as a function of momentum in the first Brillouin zone of the copper-oxide plane [frame (a)]. Constant value contours for the same quantity [frame (b)], and in frame (c) the Fermi surface for different values of second-nearest-neighbor hopping B as labeled. In all cases, the filling is fixed at $\langle n\rangle = 0.4$.

value of about 40 meV reached for $B \cong 0.25$. At still higher values of B, this frequency drops back to about 37 meV a pattern which is expected from our previous consideration of Fig. 6. It is quite clear from this figure that the gap maximum seen in the Raman spectrum is not representative of the maximum gap in the Brillouin zone and cannot be expected to scale exactly with T_c value. Instead, it is related more to the values of the gap on or near the Fermi contours. For the case $\langle n\rangle = 0.4$ and $B = 0$, this contour does not pass close to the region where the gap is maximum in the Brillouin zone and the frequency of the maximum in the Raman profile is only 30 meV instead of roughly 40 meV for $B = 0.25$ when the maximum gap is sampled. Thus even data on the B_{1g} mode require care in interpretation and cannot be taken as directly related to a quasiparticle density of state curve.

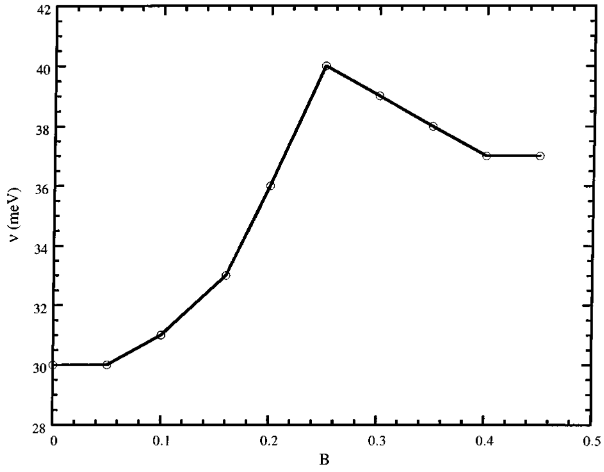

FIG. 7. The value of the frequency at the gap maximum in the B_{1g} Raman cross section as a function of B, the second-nearest-neighbor hopping parameter for fixed filling $\langle n\rangle = 0.4$ and fixed value of critical temperature $T_c = 100$ K.

IV. CONCLUSION

Within a BCS model for the pairing in a nearly antiferromagnetic Fermi liquid based on the phenomenological electron-spin susceptibility of Millis, Monien, and Pines[26] which gives a gap with $d_{x^2-y^2}$ symmetry, we have calculated the Raman susceptibility. Various photon configurations were considered and the Raman profile compared with the corresponding quasiparticle density of states. It was found that the B_{1g} spectrum bares the most resemblance to the density of state exhibiting a clear gap maximum and also showing the van Hove singularity usually at higher energies. By changing the filling from the underdoped regime to the overdoped case, we have seen the gap maximum merge with the Van Hove singularity right at optimum doping. At this point, the intensity of the gap peak is greatest and its position is very nearly at twice the value of the position of the gap peak in the density of state. The B_{2g} and screened A_{1g} modes do not allow such a simple and pleasing interpretation because of the very different weighting provided by the square of the Raman vertex. This factor strongly determines the shape of the resulting spectrum.

Depending on the shape of the Fermi surface, the Raman vertices may be more heavily weighted in different parts of the Brillouin zone. The vertex peaks may not be located near the gap maxima in k space, thus the maximum gap in the Brillouin zone may not be as significantly sampled in the Raman spectra as it is in the quasiparticle density of states. Comparison with existing data show agreement with some of the predicted features and strong disagreements with others. We have also noted that details of the band structure can strongly affect the magnitude of the A_{1g} mode when screening is included.

ACKNOWLEDGMENTS

This work was partially supported by NSERC, the Natural Sciences and Engineering Research Council of Canada, and by CIAR, the Canadian Institute for Advanced Research. We thank Tom Devereaux, Chuck Irwin, and Chris Kendziora for helpful discussions and Axel Hoffmann for discussions and sending us his thesis.

---

[1] A. A. Maksimov, A. V. Puchkov, and I. I. Tartakovskii, Solid State Commun. **81**, 407 (1992).

[2] M. Boekholt, A. Hoffmann, and G. Güntherodt, Physica C **175**, 127 (1991).

[3] D. Reznik *et al.*, Phys. Rev. B **48**, 7624 (1994).

[4] X. K. Chen, E. Altendorf, J. C. Irwin, R. Liang, and W. Hardy, Phys. Rev. B **48**, 10 530 (1993).

[5] For a more complete list, see Refs. 1–19 in Ref. 25.

[6] T. Staufer, R. Newetchek, R. Hackl, P. Müller, and H. Veith, Phys. Rev. Lett. **68**, 1069 (1992).

[7] X. K. Chen, R. Liang, W. N. Hardy, and J. C. Irwin, J. Supercond. **7**, 435 (1994).

[8] X. K. Chen, J. C. Irwin, R. Liang, and W. N. Hardy, Physica C **227**, 113 (1994).

[9] T. P. Devereaux, D. Einzel, B. Stadlober, and R. Hackl, Phys. Rev. Lett. **72**, 291 (1994).

[10] Axel Hoffmann, Ph.D. thesis, University of Aachen, 1994.

[11] A. Hoffmann, P. Lemmens, G. Güntherodt, V. Thomas, and K. Winzer, Physica C **235-240**, 1897 (1994).

[12] A. Hoffmann, P. Lemmens, L. Winkeler, and G. Güntherodt, J. Low Temp. Phys. **99**, 201 (1995).

[13] C. Kendziora and A. Rosenberg, Phys. Rev. B **52**, R9867 (1995).

[14] X. K. Chen, J. C. Irwin, H. J. Trodahl, T. Kimura, and K. Kishio, Phys. Rev. Lett. **73**, 3615 (1994).

[15] A. A. Abrikosov and L. A. Fal'kovsky, Sov. Phys. JETP **13**, 179 (1961).

[16] A. A. Abrikosov and V. M. Genkin, Sov. Phys. JETP **38**, 417 (1974).

[17] M. V. Klein and S. B. Dierker, Phys. Rev. B **29**, 4976 (1984).

[18] A. Zawadowski and M. Cardona, Phys. Rev. B **42**, 10 732 (1990).

[19] H. Monein and A. Zawadowski, Phys. Rev. B **41**, 8798 (1990).

[20] M. C. Krantz and M. Cardona, Phys. Rev. Lett. **72**, 3290 (1994).

[21] V. N. Kostur and G. M. Eliashberg, JETP Lett. **53**, 391 (1991).

[22] V. N. Kostur, Z. Phys. B **89**, 149 (1992).

[23] T. P. Devereaux, Phys. Rev. B **45**, 12 965 (1992); **47**, 5230 (1993).

[24] X. K. Chen and J. C. Irwin, Physica C **235-240**, 1089 (1994).

[25] D. Branch and J. P. Carbotte, Phys. Rev. B **52**, 603 (1995).

[26] A. J. Millis, H. Monien, and D. Pines, Phys. Rev. B **42**, 167 (1990).

[27] St. Lenck and J. P. Carbotte, Phys. Rev. B **49**, 4146 (1994).

[28] St. Lenck, J. P. Carbotte, and R. C. Dynes, Phys. Rev. B **49**, 6933 (1994); **49**, 9111 (1994).

[29] St. Lenck and J. P. Carbotte, J. Phys. Chem. Solids **54**, 1377 (1993).

[30] P. Monthoux, A. V. Balatsky, and D. Pines, Phys. Rev. Lett. **67**, 3448 (1991).

[31] P. Monthoux, A. V. Balatsky, and D. Pines, Phys. Rev. B **46**, 14 803 (1992).

[32] P. Monthoux and D. Pines, Phys. Rev. Lett. **69**, 961 (1992).

[33] P. Monthoux and D. Pines, Phys. Rev. B **47**, 9124 (1993).

[34] C. Zhou and H. J. Schulz, Phys. Rev. B **45**, 7397 (1992).

[35] G. Blumberg, B. P. Stojkovic, and M. V. Klein, Phys. Rev. B **52**, R15 741 (1995).

[36] O. K. Andersen *et al.*, Phys. Rev. B **49**, 4145 (1994).

[37] T. P. Devereaux, D. Einzel, B. Stadlober, and R. Hackl, Phys. Rev. Lett. **72**, 3290 (1994).

[38] T. P. Devereaux (private communication).